




Cite this: *Nanoscale*, 2018, **10**, 4415

Wavelength-tunable mid-infrared thermal emitters with a non-volatile phase changing material†

Kaikai Du,^{‡a} Lu Cai,^{‡a} Hao Luo,^a Yue Lu,^a Jingyi Tian,^a Yurui Qu,^a Pintu Ghosh,^a Yanbiao Lyu,^b Zhiyuan Cheng,^b Min Qiu^a and Qiang Li  ^{*a}

The ability to continuously tune the emission wavelength of mid-infrared thermal emitters while maintaining high peak emissivity remains a challenge. By incorporating the nonvolatile phase changing material Ge₂Sb₂Te₅ (GST), two different kinds of wavelength-tunable mid-infrared thermal emitters based on simple layered structures (GST-Al bilayer and Cr-GST-Au trilayer) are demonstrated. Aiming at high peak emissivity at a tunable wavelength, an Al film and an ultrathin (~5 nm) top Cr film are adopted for these two structures, respectively. The gradual phase transition of GST provides a tunable peak wavelength between 7 μm and 13 μm while high peak emissivity (>0.75 and >0.63 for the GST-Al and Cr-GST-Au emitters, respectively) is maintained. This study shows the capability of controlling the thermal emission wavelength, the application of which may be extended to gas sensors, infrared imaging, solar thermophotovoltaics, and radiative coolers.

Received 28th December 2017,

Accepted 28th January 2018

DOI: 10.1039/c7nr09672k

rsc.li/nanoscale

Introduction

Wavelength-tunable mid-infrared (MIR) emitters are essential devices in gas sensing,^{1,2} infrared imaging,^{3–5} and solar thermophotovoltaics.^{6,7} While quantum cascade lasers have been developed as the main wavelength-tunable MIR sources owing to their advantages of high spectral density and single-mode operation,⁸ their complex fabrication technology and accompanying high cost restrict their applications in areas with low-cost demands. In most applications where the requirements on emission intensity and bandwidth are not particularly strict, wavelength-tunable MIR thermal emitters can be advantageously exploited.⁹ However, traditional wavelength-tunable MIR thermal emitters are based on hot plates and tungsten lamps combined with wavelength-tunable spectral filters^{10,11} which make their structures complex and energy inefficient. By engineering the shape and geometric size of micro/nano-structures,^{12–22} MIR thermal emitters made of gratings,²³ photonic crystals,²⁴ metamaterials,²⁵ and photonic cavities^{26,27} are realized with near unity emissivity at a tailored wave-

length.²⁸ However, neither the emissivity nor the emission wavelength can be continuously tuned.

Thermal emitters with continuously tunable emissivity have been demonstrated based on micro/nano-structures in combination with advanced materials,²⁹ such as semiconductor quantum wells,^{30,31} graphene,³² and phase changing materials (such as VO_x³³ and Ge₂Sb₂Te₅ (GST)^{34–36}). Most of the current research studies are focused on continuous tuning of the peak emissivity. For example: (1) by changing the applied bias voltage in semiconductor quantum wells, a narrowband emission spectrum with a tunable emissivity from 0.12 to 0.81 can be realized at a fixed peak wavelength of 9.2 μm;³¹ (2) by changing the temperature of a VO_x/sapphire device, the peak emissivity of a broadband emission spectrum can be tuned from 0.2 to 1 without the change of the central wavelength;³³ (3) by changing the dielectric thickness in a metal–dielectric–metal metamaterial-based thermal emitter with rising temperature, the peak emissivity can be tuned from 0.5 to 0.81, during which the peak emission wavelength slightly changes from 4.9 μm to 5.2 μm;³⁷ (4) by controlling the phase transition process of GST, the emissivity of a GST-Au thermal emitter can be tuned from 0.2 to 1 with an accompanying wavelength shift from 8 μm to 11 μm.³⁴ However, the ability to tune the emission wavelength especially with a simultaneous high peak emissivity remains elusive.

In this paper, two wavelength-tunable MIR thermal emitters based on layered structures (GST-Al and Cr-GST-Au) incorporating the nonvolatile phase changing material GST are demonstrated. Aiming at high peak emissivity at a tunable wavelength, an Al and an ultrathin (~5 nm) top Cr film are adopted

^aState Key Laboratory of Modern Optical Instrumentation, College of Optical Science and Engineering, Zhejiang University, 310027 Hangzhou, China.

E-mail: qiangli@zju.edu.cn

^bInstitute of Microelectronics and Nanoelectronics, College of Information Science & Electronic Engineering, Zhejiang University, 310027 Hangzhou, China

†Electronic supplementary information (ESI) available. See DOI: 10.1039/c7nr09672k

‡These authors contributed equally to this work.

for these two structures, respectively. By controlling the intermediate phases of GST from amorphous GST (termed aGST) to crystalline GST (termed as cGST), the peak emission wavelength is continuously tuned for the wavelength range from 7 μm to 13 μm while a high peak emissivity (over 0.75 and 0.63 for the two thermal emitters, respectively) is maintained. These wavelength-tunable MIR thermal emitters offer several distinct advantages: (i) a wide wavelength-tuning range with a simultaneous high peak emissivity, which is realized by controlling the intermediate phases of GST in the designed layered structures; (ii) zero static power consumption because the GST is quite stable at room temperature and needs no extra source to maintain a certain phase; (iii) low-cost and large-scale fabrication as the layered design of the thermal emitters involves only film deposition for the fabrication.

Results and discussion

The schematic diagrams of the two kinds of wavelength-tunable MIR thermal emitters (GST-Al and Cr-GST-Au) are presented in Fig. 1. The GST-Al MIR thermal emitter is composed of a 40 nm-thick Al layer and a 450 nm-thick GST layer (Fig. 1a). For the Cr-GST-Au MIR thermal emitter, the 450 nm-thick GST layer is sandwiched between a 5 nm-thick Cr layer and an 80 nm-thick Au layer (Fig. 1b). The SEM images of the cross-section and top view (Fig. 1) are also provided.

According to Kirchhoff's law of thermal emission, the thermal emission performance of the MIR thermal emitters can be designed and studied by analyzing their absorption. The absorption properties of the GST-Al and Cr-GST-Au structures are simulated with the commercial COMSOL Multiphysics software. The proportion of amorphous atoms in the GST changes gradually as the phase transition between the amorphous and crystalline phases of GST is gradual. When the amorphous proportion is termed X , the complex refractive index of the intermediate GST can be approximately calculated as $N_x = X \times N_a + (1 - X) \times N_c$ based on Birchak's mixing rule,³⁸ where N_a and N_c are the complex refractive indices of aGST and cGST,³⁴ respectively. The refractive indices of the Al, Cr and Au films in the simulation are derived from the ellipsometer and the reference,³⁹ respectively.

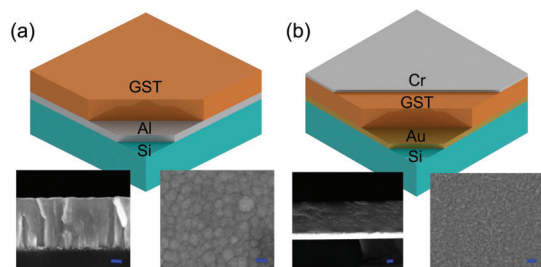


Fig. 1 Schematic diagrams and SEM images (both cross section and top view) of (a) the GST-Al and (b) the Cr-GST-Au MIR thermal emitters. The scale bar in the SEM images is 100 nm.

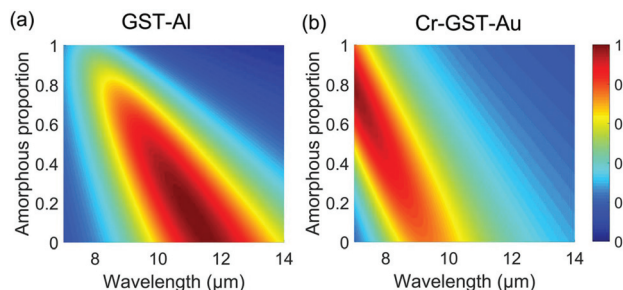


Fig. 2 The simulated absorptivity of the (a) GST-Al and (b) Cr-GST-Au MIR thermal emitters for the wavelength range from 7 μm to 13 μm when varying the amorphous proportion from 0 to 1. The thickness of GST is 450 nm and the bottom metal is 100 nm in both structures. The surface Cr layer is 5 nm-thick in the Cr-GST-Au MIR thermal emitter.

The simulated absorptivities of the GST-Al and Cr-GST-Au structures as a function of amorphous proportion and wavelength are studied (Fig. 2). For the GST-Al structure, the peak absorption wavelength is 7.92 μm at $X = 1$ (amorphous phase) and increases to 11.6 μm when X decreases to 0 (crystalline phase). The peak absorptivity remains above 0.4 during the whole phase transition process. For the Cr-GST-Au structure, the peak absorption wavelength shifts from 6.34 μm to 9.28 μm when X is decreased from 1 to 0. During the wavelength shift, the peak absorptivity maintains over 0.75. Both structures realize a tunable absorption wavelength with a simultaneous high peak absorptivity by changing the amorphous proportion of GST. Although the simulation is performed for normal incidence, it should be mentioned that the absorptivities of GST-Pt and Au-GST-Au structures also present a high robustness at an oblique incidence (Fig. S1†).

To reveal the physics behind the wavelength tunability of the GST-Al and Cr-GST-Au samples, the normalized electric field ($|E|$) and resistive loss (Q) distributions at the peak absorption wavelength for both amorphous and crystalline GST are investigated (Fig. 3). The resistive loss is related to the electric field intensity by $Q = \pi c \epsilon_0 \epsilon''(\lambda) |E|^2 / \lambda$, where $\epsilon''(\lambda)$, c , and ϵ_0 are the imaginary part of the material complex refractive index, the light velocity in a vacuum, and the vacuum permittivity, respectively. The interface reflectivity between the two films follows the Fresnel formula $R = |(\tilde{n}_2 - \tilde{n}_1) / (\tilde{n}_2 + \tilde{n}_1)|^2$, where \tilde{n}_1 and \tilde{n}_2 are the complex refractive indices ($\tilde{n} = n + ik$, where n and k denote the refractive index and extinction coefficient, respectively) of the two films, respectively.

In the GST-Al structure, the GST layer plays the role of an antireflection coating. Al is not a perfect electric conductor (PEC) and the reflection at the Al-GST interface is thereby small resulting in strong electric field penetration into the Al film (Fig. 3a and b) and the corresponding large resistive loss (Fig. 3e and f) in the Al film. As aGST is transparent at 6–14 μm , the resistive loss occurs in the Al layer in the aGST-Al structure, and 40% of the incident energy is absorbed (Fig. 3e). For the cGST-Al structure, 84.0% and 15.3% of the incident energy are absorbed by the cGST layer and the Al layer, respectively (Fig. 3f). The absorption wavelengths of

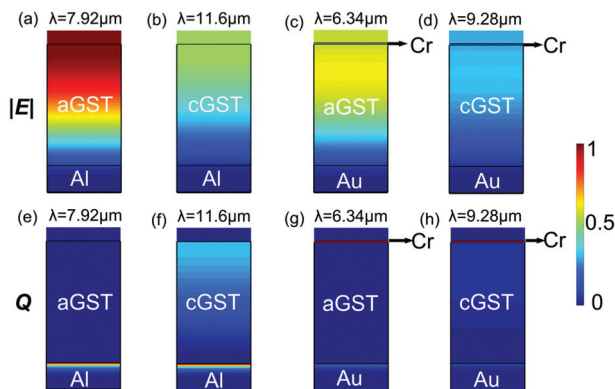


Fig. 3 The normalized electric field and resistive loss in the GST-Al and Cr-GST-Au MIR thermal emitters at the peak absorption wavelength for amorphous and crystalline GST phases. The normalized electric field distributions (a–d) and resistive loss distributions (e–h) are presented for (a, e) aGST-Al, (b, f) cGST-Al, (c, g) Cr-aGST-Au, and (d, h) Cr-cGST-Au structures. The resistive loss in the top Cr layer in (g) and (h) is not normalized as its intensity is far stronger than that in other parts.

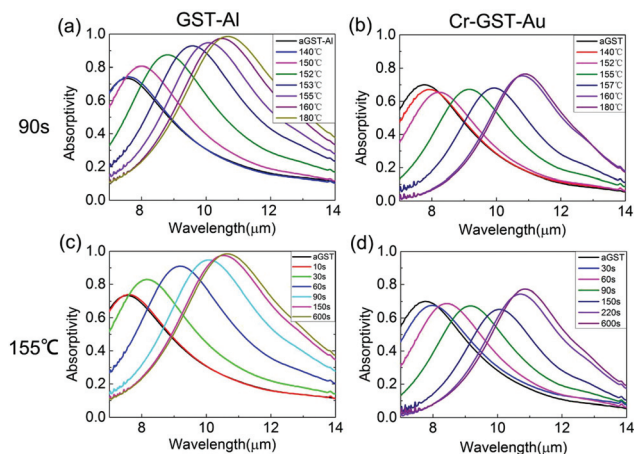


Fig. 4 The measured absorptivity curves for the MIR thermal emitters with two different annealing processes. (a) and (b) are for GST-Al and Cr-GST-Au structures annealed for 90 s at different annealing temperatures, respectively. (c) and (d) are for GST-Al and Cr-GST-Au structures annealed at 155 °C for different annealing periods, respectively.

both aGST-Al and cGST-Al structures are determined by the asymmetric Fabry–Pérot resonances, the absorptivity increases with the phase changing process owing to the increase in dielectric loss.

In the Cr-GST-Au structure, an ultrathin (~ 5 nm) Cr layer is coated on top of the GST film. The incident light can tunnel through this ultrathin metal film which makes it different from conventional bulk metals and thick metallic films with high reflectivity. The electric field is also enhanced by the symmetric FP resonance formed with the thick Au layer in the bottom and the ultrathin Cr film. The strong electric field leads to a strong resistive loss in the 5 nm-thick Cr layers (the resistive loss in the Cr layers shown in Fig. 3g and h is so high that it is not normalized to distinguish the resistive loss distribution in other layers). The 5 nm-thick Cr layers of Cr-aGST-Au and Cr-cGST-Au structures absorb 92.4% and 37.3% of the incident light, respectively. The bottom Au layers of Cr-aGST-Au and Cr-cGST-Au structures absorb 7.3% and 3.8% of the incident light, respectively. The lossy cGST absorbs 34.6% of the incident light in the Cr-cGST-Au structure.

The experimental performance of the devices is further investigated corresponding to the theoretical results discussed above. The fabrication process of the samples and the measurement methods are introduced in the experimental methods section. The GST-Al and Cr-GST-Au samples with different amorphous proportions of GST are prepared with thermal annealing. Two distinct annealing methods are adopted to tune the amorphous proportion of GST: applying either different annealing temperatures or different annealing times. For different annealing temperatures on different samples at a fixed annealing time ($t = 90$ s), the absorption performance of the GST-Al (Fig. 4a) and Cr-GST-Au (Fig. 4b) samples changes with the annealing temperature. The peak absorption wavelength of the GST-Al samples shifts from 7.59 μm to 10.7 μm . The maximum peak absorptivity is 0.99

and the minimum is above 0.73. Similarly, for the Cr-GST-Au sample, the peak absorption wavelength shifts from 7.75 μm to 10.9 μm with the peak absorptivity over 0.63 when the annealing temperature is increased. Different samples were annealed for different times at a fixed annealing temperature ($T = 155$ °C). A similar shift in both peak absorption wavelength and peak absorptivity for both GST-Al and Cr-GST-Au samples can be seen in Fig. 4c and d. A long annealing time results in a reduced amorphous proportion contributing to the red-shift of the peak absorption wavelength. Both of these annealing methods can be implemented to realize wavelength tunable absorption with a simultaneous high peak absorptivity for both GST-Al and Cr-GST-Au structures. It is observed that the peak absorption wavelength red shifts in both simulated and experimental results (Fig. 2 and 4). The differences of the peak absorptivity and wavelength in between are owing to the roughness of the films and the insufficient accuracy of the refractive indices in the simulation compared with the materials in the experiments.

The emission power of the GST-Al and Cr-GST-Au MIR thermal emitters is further measured with FTIR. The emission power is measured at 100 °C and black soot is adopted as a reference. The peak emission wavelength for both the GST-Al (Fig. 5a) and Cr-GST-Au (Fig. 5b) MIR thermal emitters shifts to a longer wavelength when the annealing temperature for GST is increased with a fixed annealing time ($t = 90$ s). During the wavelength shift, the emission power remains high for both structures. Wavelength-tunable thermal emission can also be realized for both the GST-Al (Fig. 5c) and Cr-GST-Au (Fig. 5d) MIR thermal emitters by increasing the annealing time with a fixed annealing temperature ($T = 155$ °C). The measured emission power of the samples fits well with the measured absorptivity (Fig. 4). The experimental results demonstrate that the emission wavelength can be tuned simply by controlling the annealing time and temperature,

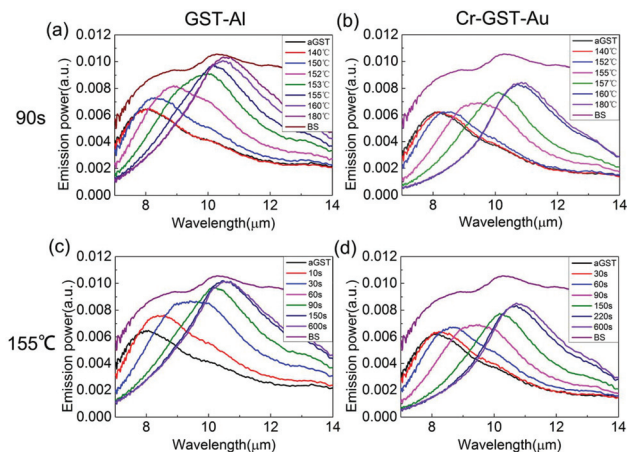


Fig. 5 The measured thermal emission power at 100 °C for the MIR thermal emitters with different annealing times and temperatures. (a) and (b) are GST-Al and Cr-GST-Au MIR thermal emitters annealed at different temperatures ($t = 90$ s), respectively. (c) and (d) are GST-Al and Cr-GST-Au MIR thermal emitters annealed at different times ($T = 155$ °C), respectively.

which, in turn, provides new avenues for flexibly tuning the thermal emission wavelength.

We have demonstrated two kinds of wavelength-tunable (7 μm –13 μm) MIR thermal emitters with GST-Al and Cr-GST-Au structures. We further discuss the influence of geometric parameters, the choice of metallic materials, and the annealing process on the performances of the MIR thermal emitters:

(1) Geometric parameters: The thickness of the GST layer is set as 450 nm. The Cr layer is set as 5 nm, which is optimized for the continuous film with high absorptivity of Cr-aGST-Au (Fig. S2†). The emission wavelength increases with the GST thickness in both the MIR thermal emitters; the tunable thermal emission wavelength range can thereby be further expanded (Fig. S3–S7†).

(2) Choice of metallic materials: In the GST-Al MIR thermal emitter, Al is chosen because of its index matching with GST which induces low reflection and thereby high absorption. The Al can be replaced by other materials with low extinction coefficient (such as Ni, Cr, *etc.*), and a similar wavelength-tunable absorptivity/emissivity can be realized. In the Cr-GST-Au thermal emitter, the strong electric field intensity in the top ultrathin metallic film dominates the absorption. Therefore, a similar wavelength-tunable absorptivity/emissivity can also be obtained by replacing the metals (for both top and bottom materials) with other metals (such as Pt, Al, Ag, *etc.*).

(3) Annealing process: The annealing for crystallization has been demonstrated by either increasing the temperature with a constant time ($t = 90$ s) or increasing the time while keeping the temperature ($T = 155$ °C) fixed. The crystallization rate of GST depends on the annealing temperature, and therefore the time span in the latter case can be decreased if the annealing temperature is higher than 155 °C. The reamorphization of GST, which can be implemented at a temperature above

640 °C, is not demonstrated owing to the low melting point of Al and Au films at the nanoscale. Refractory metals (such as W, Mo, *etc.*) can be exploited to stand the reamorphization temperature. Besides thermal annealing, the phase transition process can also be realized by laser pulses^{40–42} and electrical stimulations⁴³ which can shorten the annealing timescale to nanoseconds or even femtoseconds.

Experimental methods

Fabrication of the samples

The GST-Al and Cr-GST-Au MIR thermal emitters are fabricated with the film deposition methods. The fabrications start with the deposition of optically thick Al (40 nm) and Au (80 nm) films by magnetron sputtering, respectively. A 450 nm-thick GST film is then deposited using magnetron sputtering with the alloy ($\text{Ge}_2\text{Sb}_2\text{Te}_5$) target. A 5 nm-thick Cr film is deposited on the GST film for the Cr-GST-Au structure.

Annealing of the samples

The as-deposited aGST can be gradually crystallized by different annealing processes, which is implemented on a temperature-controlled hot plate. Two annealing methods are adopted to control the phase transition process for wavelength-tunable emission: (i) the annealing temperature is varied (100 °C–180 °C) while the annealing time is kept at 90 s and (ii) varying the annealing time (10 s–600 s) while keeping the annealing temperature fixed at 155 °C.

Absorptivity measurements

As the bottom Al and Au films are optically thick, the transmission can be neglected. The absorptivity (A) can thus be derived on the basis of the measured reflectivity (R) by $A = 1 - R$. The reflection spectra are recorded by using the Hyperion 1000 infrared microscope equipped with a liquid-nitrogen-refrigerated MCT detector.

Emissivity measurements

In the emissivity measurement, the GST-Al sample, the Cr-GST-Au sample, and the black soot are separately fixed on a hot plate whose temperature is fixed at 100 °C. The thermal emissivity is measured with a Fourier transform infrared spectrometer (FTIR), Bruker Vertex 70, equipped with a DTGS detector. Black soot is chosen as the reference owing to its high emissivity close to an ideal black body. The black soot reference is made by firing a steel slice with a candle. The emissivity of a sample can be derived by normalizing the measured emission power with that of the black soot at the same temperature (100 °C).

Conclusions

In summary, two different kinds of thermal emitters based on GST-Al and Cr-GST-Au structures with simultaneous wave-

length tunability and high peak emissivity are introduced. For the GST-Al structure, the antireflection performance of GST for metals with index matching leads to large light penetration and high emissivity. For the Cr-GST-Au structure, the enhanced electric field in the ultrathin top Cr layer by the tunneling effect contributes to the high emissivity. A tunable emission wavelength between 7 μm and 13 μm with sustained high emissivity is achieved by controlling the gradual phase transition of GST. The peak emissivity of the two MIR thermal emitters remains above 0.73 and 0.63 when the peak wavelength is varied. The GST phases are stable at room temperature and therefore the two wavelength-tunable MIR thermal emitters feature zero-static-power. Moreover, these devices have the advantages of large-area and lithography-free fabrication. Combining all the advantages, these MIR thermal emitters can control the thermal emission wavelength simultaneously with high emissivity and thereby have many potential applications including chemical composition analysis, thermophotovoltaics, and radiative coolers.

Conflicts of interest

There are no conflicts to declare.

Author contributions

Q. Li and M. Qiu designed and guided the study. K. Du, L. Cai, H. Luo, Y. Lu, Y. Lyu and Z. Cheng performed the fabrication of samples. K. Du, L. Cai, H. Luo, Y. Lu and Y. Qu measured the infrared spectra of the samples. K. Du, J. Tian, P. Ghosh, M. Qiu and Q. Li analysed the theoretical principles. K. Du, L. Cai, P. Ghosh and Q. Li wrote the manuscript with input and contributions from all the co-authors. All authors have given approval to the final version of the manuscript.

Acknowledgements

This work is supported by the National Key Research and Development Program of China (No. 2017YFA0205700) and the National Natural Science Foundation of China (Grant No. 61425023, 61575177 and 61775194).

Notes and references

- J. Hodgkinson and R. P. Tatam, *Meas. Sci. Technol.*, 2012, **24**, 12004.
- A. Lochbaum, Y. Fedoryshyn, A. Dorodnyy, U. Koch, C. Hafner and J. Leuthold, *ACS Photonics*, 2017, **4**, 1371.
- J. K. Coulter, C. F. Klein and J. C. Jafolla, *Proc. SPIE*, 2002, **4708**, 354.
- Y. Rauste, E. Herland, H. Frelander, K. Soini, T. Kuoremaki and A. Ruokari, *Int. J. Remote Sens.*, 2010, **18**, 2641–2656.
- L. J. Jiang, E. Ng, A. Yeo, S. Wu, F. Pan, W. Y. Yau, J. H. Chen and Y. Yang, *Int. J. Biomed. Eng. Technol.*, 2005, **29**, 257–267.
- A. Lenert, D. M. Bierman, Y. Nam, W. R. Chan, I. Celanović, M. Soljačić and E. N. Wang, *Nat. Nanotechnol.*, 2014, **9**, 126–130.
- E. Rephaeli and S. Fan, *Opt. Express*, 2009, **17**, 15145–15159.
- J. Faist, F. Capasso, D. L. Sivco, C. Sirtori, A. L. Hutchinson and A. Y. Cho, *Science*, 1994, **264**, 553–556.
- P. Barritault, M. Brun, S. Gidon and S. Nicoletti, *Sens. Actuators, A*, 2011, **172**, 379–385.
- S. Z. Ali, A. D. Luca, R. Hopper, S. Boual, J. Gardner and F. Udrea, *IEEE Sens. J.*, 2015, **15**, 6775–6782.
- A. Vorobyev, V. Makin and C. Guo, *Phys. Rev. Lett.*, 2009, **102**, 234301.
- K. A. Arpin, M. D. Losego, A. N. Cloud, H. Ning, J. Mallek, N. P. Sergeant, L. Zhu, Z. Yu, B. Kalanyan and G. N. Parsons, *Nat. Commun.*, 2013, **4**, 2630.
- W. Streyer, K. Feng, Y. Zhong, A. J. Hoffman and D. Wasserman, *Appl. Phys. Lett.*, 2015, **107**, 81105.
- J. A. Schuller, T. Taubner and M. L. Brongersma, Optical antenna thermal emitters, *Nat. Photonics*, 2009, **3**, 658–661.
- C. Fu and Z. M. Zhang, *Front. Energy Power Eng. China*, 2009, **3**, 11–26.
- D. Costantini, A. Lefebvre, A. L. Coutrot, I. Moldovan-Doyen, J. P. Hugonin, S. Boutami, F. Marquier, H. Benisty and J. J. Greffet, *Phys. Rev. Appl.*, 2015, **4**, 14023.
- S. Han, J. Shin, P. Jung, H. Lee and B. J. Lee, *Adv. Opt. Mater.*, 2016, **4**, 1265–1273.
- T. Yokoyama, T. D. Dao, K. Chen, S. Ishii, R. P. Sugavaneshwar, M. Kitajima and T. Nagao, *Adv. Opt. Mater.*, 2016, **4**, 1987–1992.
- P. N. Dyachenko, S. Molesky, A. Y. Petrov, M. Störmer, T. Krekeler, S. Lang, M. Ritter, Z. Jacob and M. Eich, *Nat. Commun.*, 2016, **7**, 11809.
- T. Asano, M. Suemitsu, K. Hashimoto, M. De Zoysa, T. Shibahara, T. Tsutsumi and S. Noda, *Sci. Adv.*, 2016, **2**, e1600499.
- N. N. Shi, C. Tsai, F. Camino, G. D. Bernard, N. Yu and R. Wehner, *Science*, 2015, **349**, 298–301.
- X. Zhang, H. Liu, Z. G. Zhang, Q. Wang and S. N. Zhu, *Sci. Rep.*, 2017, **7**, 41857.
- J. Greffet, R. Carminati, K. Joulain, J. Mulet, S. Mainguy and Y. Chen, *Nature*, 2002, **416**, 61–64.
- M. U. Pralle, N. Moelders, M. P. McNeal, I. Puscasu, A. C. Greenwald, J. T. Daly, E. A. Johnson, T. George, D. S. Choi, I. El-Kady and R. Biswas, *Appl. Phys. Lett.*, 2002, **81**, 4685.
- X. Liu, T. Tyler, T. Starr, A. F. Starr, N. M. Jokerst and W. J. Padilla, *Phys. Rev. Lett.*, 2011, **107**, 045901.
- Z. Wang, T. S. Luk, Y. Tan, D. Ji, M. Zhou, Q. Gan and Z. Yu, *Appl. Phys. Lett.*, 2015, **106**, 101104.
- A. S. Roberts, M. Chirumamilla, K. Thilsing-Hansen, K. Pedersen and S. I. Bozhevolnyi, *Opt. Express*, 2015, **23**, 1111.
- J. Zhou, X. Chen and L. J. Guo, *Adv. Mater.*, 2016, **28**, 3017–3023.

- 29 A. Kazemi Moridani, R. Zando, W. Xie, I. Howell, J. J. Watkins and J. Lee, *Adv. Opt. Mater.*, 2017, **5**, 1600993.
- 30 M. De Zoysa, T. Asano, K. Mochizuki, A. Oskooi, T. Inoue and S. Noda, *Nat. Photonics*, 2012, **6**, 535–539.
- 31 T. Inoue, M. De Zoysa, T. Asano and S. Noda, *Nat. Mater.*, 2014, **13**, 928–931.
- 32 V. W. Brar, M. C. Sherrott, M. S. Jang, S. Kim, L. Kim, M. Choi, L. A. Sweatlock and H. A. Atwater, *Nat. Commun.*, 2015, **6**, 7032.
- 33 M. A. Kats, R. Blanchard, S. Zhang, P. Genevet, C. Ko, S. Ramanathan and F. Capasso, *Phys. Rev. X*, 2013, **3**, 41004.
- 34 K. Du, Q. Li, Y. Lyu, J. Ding, Y. Lu, Z. Cheng and M. Qiu, *Light: Sci. Appl.*, 2017, **6**, e16194.
- 35 A. Tittl, A. K. U. Michel, M. Schäferling, X. Yin, B. Gholipour, L. Cui, M. Wuttig, *et al.*, *Adv. Mater.*, 2015, **27**, 4597–4603.
- 36 Y. Qu, Q. Li, K. Du, *et al.*, *Laser Photonics Rev.*, 2017, **11**, 1700091.
- 37 X. Liu and W. J. Padilla, *Adv. Mater.*, 2016, **28**, 871–875.
- 38 N. V. Voshchinnikov, G. Videen and T. Henning, *Appl. Opt.*, 2007, **46**, 4065–4072.
- 39 A. D. Rakić, A. B. Djurišić, J. M. Elazar and M. L. Majewski, *Appl. Opt.*, 1998, **37**, 5271.
- 40 T. Hira, T. Homma, T. Uchiyama, K. Kuwamura, Y. Kihara and T. Saiki, *Appl. Phys. Lett.*, 2015, **106**, 31105.
- 41 P. Li, X. Yang, T. W. Maß, J. Hanss, M. Lewin, A. U. Michel, M. Wuttig and T. Taubner, *Nat. Mater.*, 2016, **15**, 807.
- 42 C. Rios, P. Hosseini, C. D. Wright, H. Bhaskaran and W. H. Pernice, *Adv. Mater.*, 2014, **26**, 1372–1377.
- 43 Y. Hu, H. Zou, J. Zhang, J. Xue, Y. Sui, W. Wu, L. Yuan, X. Zhu, S. Song and Z. Song, *Appl. Phys. Lett.*, 2015, **107**, 263105.